NANO LETTERS

2008
Vol. 8, No. 1
147−151

Correlated Random Telegraph Signal and Low-Frequency Noise in Carbon Nanotube Transistors

Fei Liu*,† and Kang L. Wang‡

IBM T. J. Watson Research Center, Yorktown Heights, New York 10598, and Department of Electrical Engineering, University of California at Los Angeles, Los Angeles, California 90095

Received September 6, 2007; Revised Manuscript Received November 6, 2007

ABSTRACT

A correlated random telegraph signal is observed from the interaction of two individual defects in a carbon nanotube transistor. It is shown that the amplitude fluctuation of one defect significantly depends on the state of the other defect. Moreover, statistics of the correlated switchings is shown to deviate from the ideal Poisson process. Physics of this random telegraph signal correlation is attributed to the fact that the two defects are located closer than the sum of their Fermi–Thomas screening lengths. This work brings new implications to the source of low frequency noise in nanodevices. Moreover, statistic studies provide a new avenue to study correlated effects due to particle interactions.

Variability becomes a critical issue for the performance of scaled metal oxide semiconductor field effect transistors (MOSFETs) and other integrated nanodevices.[1] Charge fluctuations often result in noise, particularly low frequency noise, appearing as $1/f$ noise and/or random telegraph signals (RTSs).[2] As studied extensively,[3] the $1/f$ noise and RTSs in scaled MOSFETs and nanotransistors (carbon nanotube field effect transistors (CNT-FETs) and other kinds of nanowire transistors) are attributed to charge fluctuations of charging and discharging of individual defects, which comes mainly from the interface dangling bonds located between semiconductors and the oxide gate stacks.[4,5,6,7] As devices shrink, the low frequency noise of scaled MOSFETs and nanodevices begins to deviate from the $1/f$ characteristics. This phenomenon suggests that the ensemble average of random telegraph signals resulted from trapping events, which gives rise to $1/f$ noise, is no longer valid;[8] therefore, the statistical nature of individual RTSs and the correlation properties need to be addressed in order to further understand noise behavior in nanodevices. CNT-FETs are used for the study. The understanding of individual RTSs (time domain information) and low frequency noise behavior (frequency domain information) obtained from CNT-FETs can be generalized to other nanotransistors. In this work, single-walled carbon nanotubes are made by a standard chemical vapor deposition (CVD).[9] In our previous work,[8] we discussed a four-level uncorrelated RTS. In this work, we report the first observation of a correlated RTS due to two individual defects. Moreover, three statistic algorithms, full counting probability function statistics,[10,11] dwell time statistics,[12] and noise power spectrum, are used for data analysis. Our statistic results from the RTS show the deviation from the ideal (random and uncorrelated) Poisson process. This further confirms correlations among several defects/traps. The observation of correlated RTS due to two individual defects provides insight into the fundamental physical mechanism of noise and offers a new method to construct noise models for nanotransistors.

Source-drain current ($I-V$) was measured after amplification of the signals using a standard low noise operational amplifier (a bandwidth of 500 MHz) through a sampling resistor. The time domain signal after the amplification is captured by a 54810A Infiniium Oscilloscope (a bandwidth of 500 MHz). Figure 1a shows a RTS obtained from a CNT-FET measured at 4.2 K with a gate bias of $V_g = -1.4$ V and a source-drain bias of $V_{ds} = -99$mV. There are four major switching levels (indicated by the red dashed lines)[13] resulting from a slow switching defect C and a fast switching defect D. Physical locations of these defects and their relative energy levels are schematically shown in Figure 1b. The four current levels correspond to both defects filled (level I), defect C filled and defect D empty (level II), defect C empty and defect D filled (level III), and both defects empty (level IV), respectively. The green solid squares of Figure 2a show its current noise power spectrum density at 4.2K, two corner frequencies at 0.2 and 5.8 Hz corresponding to the slow

* To whom correspondence should be addressed. E-mail: liufe@us.ibm.com. PACS numbers: 05.40.-a, 34.10.+x.
† IBM T. J. Watson Research Center.
‡ University of California at Los Angeles.

10.1021/nl0722774 CCC: $40.75
Published on Web 12/13/2007

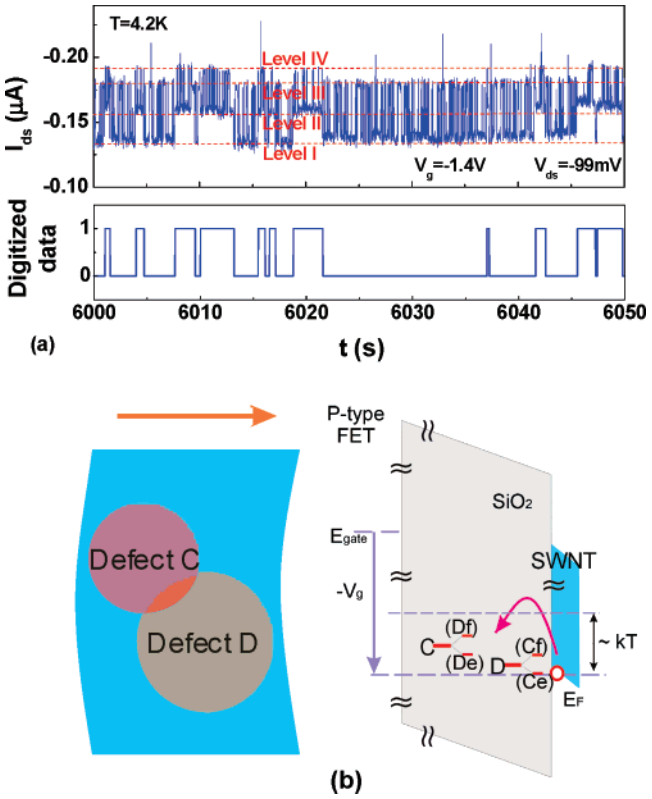

Figure 1. (a) Time dependent current of a RTS for a CNT-FET at 4.2 K biased at $V_g = -1.4$ V and $V_{ds} = -99$ mV. Four major switching levels are shown in red dashed lines due to two defect switchings (defects C and D). The slow defect (defect C) fluctuations are digitized in the bottom graph. (b) Schematic drawing of effective interaction areas of the two defects (C and D) and their relative locations in the carbon nanotube channel. Schematic drawing of relative energy of defect C and D with energy level splittings due to effective area overlap.

switchings due to defect C and the fast switchings due to defect D, respectively. Although the current difference between levels I and III is 0.045 μA, the difference between levels II and IV is 0.03 μA. This means the switching amplitude of fast defect D depends on the state of defect C, which indicates that there is an amplitude correlation between these two defects. To understand the amplitude correlation, the RTS switchings are separated according to which defect stimulates the switchings. The current correlation coefficient (r) for defect C and D switching events is obtained as[14]

$$r = \frac{\sum_{i=1}^{M}(I_i^C - \overline{I_i^C})(I_i^D - \overline{I_i^D})}{\sqrt{\sum_{i=1}^{M}(I_i^C - \overline{I_i^C})^2 \sum_{i=1}^{M}(I_i^D - \overline{I_i^D})^2}} = -0.12$$

where I_i^C and I_i^D are the ith extracted current level for defects C and D, respectively, and $\overline{I_i^C}$ and $\overline{I_i^D}$ are the average current level for C and D, respectively. M is the total number of current level measured. As an example, the bottom of Figure 1a shows the digitization for the defect C switchings, from which the full counting statistics of defect

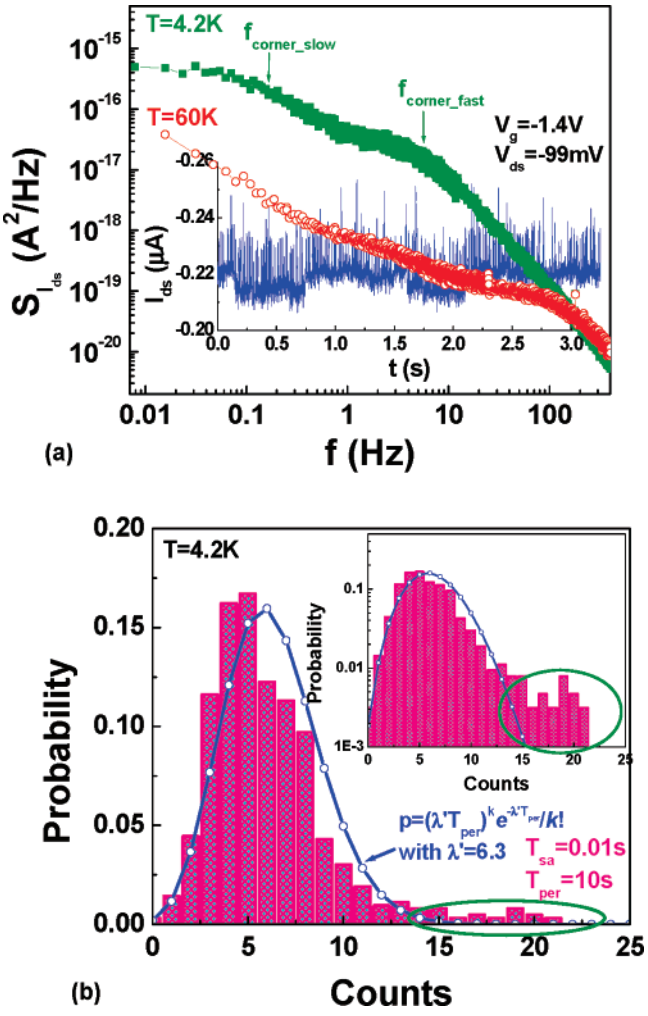

Figure 2. (a) Noise power spectrum density measured with $V_g = -1.4$ V and $V_{ds} = -99$ mV at 4.2 K (green solid squares) and 60 K (red open dots), respectively. The inset shows the time domain current data at 60 K. (b) Full counting probability function for defect C transitioning from the empty state to the filled state in 10 s (T_{per}) at 4.2 K. The measured distribution deviates significantly from Poisson distribution (fitted with the measured expectation value). The inset shows the same full counting probability function in a semilogarithmic scale to highlight the tail in the large count portion.

C, shown in Figure 2b, is obtained for the transition from 1 to 0 during a time period (T_{per}) of 10 s. Because T_{sa} (0.01 s) $\approx 1/160\tau_c$ (1.6 s), where T_{sa} is the sampling time and τ_c is the capture time of the defect, the statistic errors due to the finite sampling time are ignorable as shown in ref 12. More precisely, if a standard chi-square test is used for the full counting statistics,[15] null hypothesis that the measured statistics with $T_{sa} \approx 1/160\tau_c$ follows Poisson statistics should be retained with a significant level of 0.01. However, interestingly, the statistics of defect C significantly departs from the ideal Poisson distribution. The null hypothesis that measured full counting statistics from defect C follows Poisson statistics and is rejected at any reasonable significant level. Such a derivation from the Poisson distribution suggests a correlation in the transition rates for defects C and D.

In the following, a model based on Fermi−Thomas model[16] is given to explain the defect correlation in both

amplitude and statistics as observed in the experiment. Here, each individual defect fluctuation has an effective interaction area, within which the local potential could be affected by the charging of the defects.[17] If the defects are located close to the SWNT/oxide interface, the radiuses of the effective interaction areas equal to the Fermi−Thomas screening length at low temperature.[15,18] When the distance between these two defects C and D is smaller than the summation of the two Fermi−Thomas screening lengths as shown in Figure 1b, the correlation between the defect centers could be observed in both the RTS amplitude and the RTS statistics.

Based on this model, it is known that charging and discharging of either of the two defects can modulate the local potential and thus channel carrier mobility and channel carrier density in the overlap range area. When defect C (or D) is charged, the effective channel width decreases. As a result, the portion of the modulation due to defect D (or C) becomes larger, resulting in larger RTS amplitude for defect D (or C) (shown in Figure 1a). This is opposite to the case that two defects are far away from each other, where the switching amplitude of one RTS is larger when the total current is larger. The latter case is because a larger current modulation happens when there is larger current passing through the defect, i.e., when the other defect is not charged. Also, it is worth noting that the switching amplitude difference of defect D becomes less dependent on defect C when the temperature increases from 4.2 to 60 K, as can be seen from the inset of Figure 2a. The RTS data indicates less amplitude correlation between the two defects C and D at the higher temperature of 60 K. Such an observation is consistent with the fact that the screening length decreases with the carrier density increase which is indicated by the larger source-drain current at a higher temperature.

Moreover, statistics correlation of the RTS is directly proportional to the overlap area. The filled state energy level (or the empty state energy level) for defect C is different when defect D is filled or empty, and so does defect D when defect C is in a different state. The statistics of defect D are summarized in Figure 3a,b using the full counting statistics and dwell time statistics (plotted in a semilogarithmic scale). The data are obtained from a faster time measurement with $T_{sa} = 0.002$ s (not shown here). The sampling time is 17 times longer than the switching time constants of defect D, suggesting an error of less than 4%. Because the deviation from the ideal Poisson distribution is much larger than 4%, we do not correct the error caused by finite sampling time for simplification. For defect D, the full counting statistics and the dwell time statistics are obtained for the following three cases: (1) ${}^{f}\tau_c^{Cf} = 0.041$ s (in Figure 4a) and ${}^{dw}\tau_c^{Cf} = 0.043$ s (in Figure 4b) for defect C in the filled state shown in red curves, (2) ${}^{f}\tau_c^{Ce} = 0.033$ s and ${}^{dw}\tau_c^{Ce} = 0.039$ s for defect C in the empty state shown in blue curves, and (3) ${}^{f}\tau_c = 0.036$ s and ${}^{dw}\tau_c = 0.041$ s for the combined statistics regardless of the state of defect C shown in green curves. The superscripts Cf and Ce represent defect C in the filled and empty states, respectively. It is shown that substantial modification in the statistics of defect D could be observed due to the state of defect C. According to the detailed balance

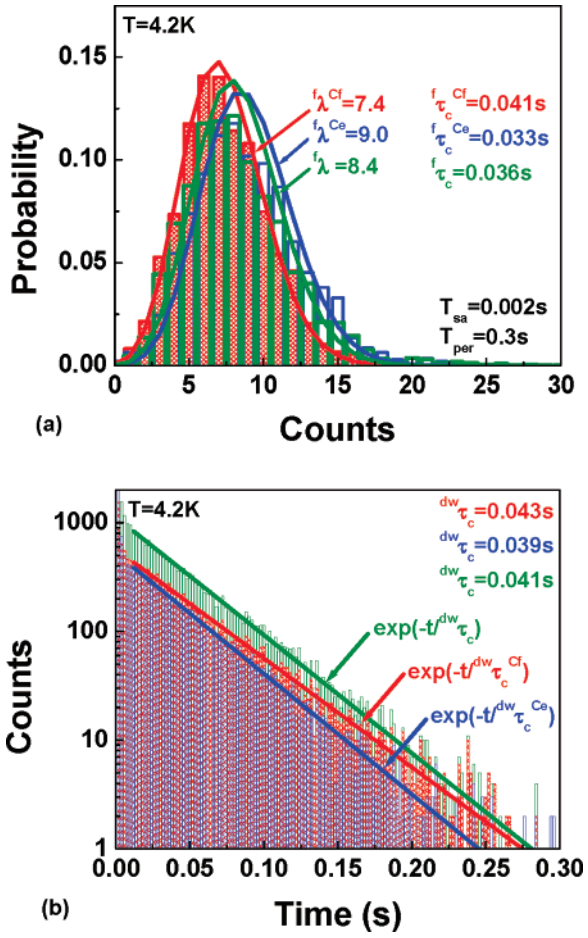

Figure 3. (a) Full counting probability function for fast defect D transitioning from the empty state to the filled state in 0.3 s (T_{per}) at 4.2 K for three cases: defect C in the filled state (shown in red), defect C in the empty state (shown in blue), and the combined statistics regardless of the state of defect C (shown in green). The superscripts Cf and Ce represent defect C in the filled and the empty states, respectively. (b) The counts of the time duration for the next time that defect D is filled in a semilogarithmic plot for the above three cases in (a).

relation,[19] the capture/emission ratio of a defect state for a hole is $\tau_c/\tau_e = g\ \exp(E_T - E_F/k_BT)$, where g is the energy degeneracy of the trap, E_T is the defect energy, E_F is the Fermi energy of the SWNT, k_B is the Boltzmann constant, and T is the carrier temperature. With the assumption that the carrier temperature is close to the ambient temperature (4.2 K) for $V_{ds} = -99$ mV, the energy splitting of defect D when defect C is filled ($E_T^{D(Cf)}$) or empty ($E_T^{D(Ce)}$) can be obtained from the fast sampling data (not shown here)

$$E_T^{D(Cf)} - E_T^{D(Ce)} = k_B T\left(\ln\left(\frac{1}{g}\cdot\frac{\tau_c}{\tau_e}\right)^{Cf} - \ln\left(\frac{1}{g}\frac{\tau_c}{\tau_e}\right)^{Ce}\right) \approx 0.03\ \text{meV} \quad (1)$$

Similarly, the energy splitting for defect C is

$$E_T^{C(Df)} - E_T^{C(De)} = k_B T\left(\ln\left(\frac{1}{g}\cdot\frac{\tau_c}{\tau_e}\right)^{Df} - \ln\left(\frac{1}{g}\frac{\tau_c}{\tau_e}\right)^{De}\right) \approx 0.14\ \text{meV} \quad (2)$$

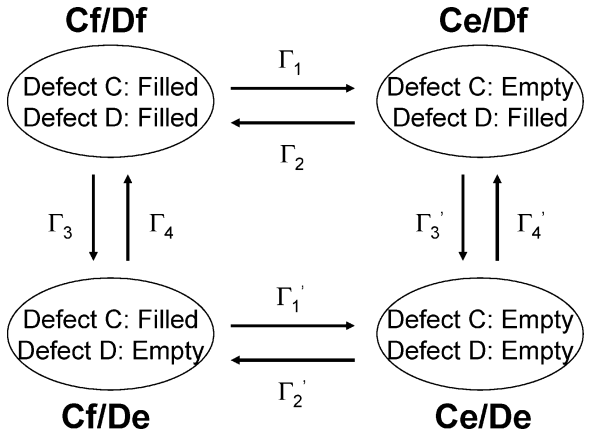

Figure 4. Schematic state diagram for the two correlated defects. The four states Cf/Df, Ce/Df, Cf/De, and Ce/De correspond to: both defects C and D filled, defect C empty and defect D filled, defect C filled and defect D empty, and both the defects C and D empty. The probabilities for the four states are $P_{Cf/Df}$, $P_{Ce/Df}$, $P_{Ce/De}$, and $P_{Cf/De}$, respectively. Γ_1, Γ_2, Γ_3, Γ_4, Γ_1', Γ_2', Γ_3', and Γ_4' are the transition rates between the different states.

The energy splitting and the probability distribution deviation are due to the interaction of defect D and defect C in the overlap area. By comparing Figure 2b with Figure 3a, it is clear that the larger energy splitting for defect C with respect to defect D results in a larger derivation from Poisson distribution.

To understand how the defect interaction affects the RTS statistics, the RTS transition is modeled by a Markov chain. As shown in Figure 4, the Markov chain has four states: Cf/Df, Ce/Df, Cf/De, and Ce/De. The probabilities for the four states are denoted by $P_{Cf/Df}$, $P_{Ce/Df}$, $P_{Ce/De}$, $P_{Cf/De}$, respectively. Note that Γ_1 (Γ_1') is the transition rate for defect C from filled to empty when D is filled (empty). Γ_1 and Γ_1' are generally different as known from the previous discussion. We assume that simultaneous two-particle-transition from Cf/Df to Ce/De or from Ce/Df to Cf/De is negligible. Therefore, the transition rate equations are

$$\begin{aligned}\dot{P}_{Cf/Df} &= -P_{Cf/Df}\Gamma_1 - P_{Cf/Df}\Gamma_3 + P_{Cf/De}\Gamma_4 \\ \dot{P}_{Cf/De} &= -P_{Cf/De}\Gamma_4 - P_{Cf/De}\Gamma_1' + P_{Cf/Df}\Gamma_3\end{aligned} \quad (3)$$

with the initial condition $P_{Cf/De}(0) = R$ and $P_{Cf/Df}(0) = 1 - R$. In the following, we elaborate the statistics of the defect C switching as an example. The statistics of defect D switching could be obtained similarly. By solving the rate equation, the probability density function (i.e., transition rate) of defect C from filled to empty is

$$P^{C}_{(f\to e)}(t) = a_1 \exp(-x_1 t) + a_2 \exp(-x_2 t) \quad (4)$$

where $x_{1,2} = (\Gamma_1 + \Gamma_1' + \Gamma_3 + \Gamma_4) \mp [(\Gamma_1 + \Gamma_1' + \Gamma_3 + \Gamma_4)^2 - 4(\Gamma_1\Gamma_1' + \Gamma_1'\Gamma_3 + \Gamma_1\Gamma_4)]^{1/2}/2$, $a_1 = \xi[\Gamma_1/\Gamma_3(-x_1 + \Gamma_1' + \Gamma_4) + \Gamma_1']$, $a_2 = (R - \xi)[\Gamma_1/\Gamma_3(-x_2 + \Gamma_1' + \Gamma_4) + \Gamma_1']$, and $\xi = \Gamma_3(1 - R) - R(-x_2 + \Gamma_1' + \Gamma_4)/(x_2 - x_1)$. We could obtain its corresponding complementary cumulative distribution as

$$\mathrm{CCDF}^{C}_{(f\to e)}(t) = \int_0^t P^{C}_{(f\to e)}(\tau)\,d\tau = k_1 \exp(-x_1 t) + k_2 \exp(-x_2 t) \quad (5)$$

where $k_1 = a_1/x_1$, $k_2 = a_2/x_2$, and $k_1 + k_2 = 1$. We can denote the total number of switchings during each T_{per} as $X(T_{per})$. As shown in Figure 2b, T_{per} is roughly 6 times larger than the capture time of defect C. According to ref 14, the defect C switching can be considered as a renewal stochastic process. By using the asymptotic property of the renewal process theory, the variance-to-expectation value-ratio of the full counting statistics for defect C (shown in Figure 2b) due to the presence of the other close defect D is

$$\frac{\mathrm{Var}[X(T_{per})]}{E[X(T_{per})]} = \frac{\dfrac{2k_1}{\lambda_1^2} + \dfrac{2(1-k_1)}{\lambda_2^2} - \left(\dfrac{k_1}{\lambda_1} + \dfrac{1-k_1}{\lambda_2}\right)^2}{\left(\dfrac{k_1}{\lambda_1} + \dfrac{1-k_1}{\lambda_2}\right)^2} \geq \frac{\mathrm{Var}[X(T_{per})]}{E[X(T_{per})]}\Big|_{\mathrm{Poisson}} = 1 \qquad \text{as } T_{per} \to \infty \quad (6)$$

The tail of the curve in Figure 2b as highlighted by green ellipses shows a significant deviation from Poisson distribution. This is because the transition rate for defect C from filled to empty is the summation of the two different exponential components in the rate equation (as expressed in eq 4) due to the coupling between defects C and D. Therefore, the variance of the measured full counting statistics is larger than the Poisson statistics with the same expectation value (eq 6). In return, it is shown here that the statistic property of noise may be used to understand many body interactions in the condensed matter physics.

Low frequency noise spectrum of devices is Fourier transformation of time domain current autocovariance.[20,21] The understanding of the multiple defects correlation has implications on the noise behavior of devices. It is clear that the correlation between defects will affect the amplitude of current switchings and the statistics of defect switchings, and therefore the noise behavior of transistors. Traditionally, the mechanism of $1/f$ like low frequency noise in the field effect transistors is due to the summation of lots of INDEPENDENT two-level random telegraph signals with different time constants according to the McWhorter model.[22,23] As the device is scaled down, the assumption of ensemble average of random telegraph signals breaks down due to limited numbers of activated defects. In this case, low frequency noise shows Lorentzian-like distribution. In this study, however, the observed correlation among defects could be another important mechanism for low frequency noise in nanotransistors. Different noise characteristics from both $1/f$ behavior and Lorentzian-like behavior are expected due to the correlated property of noise sources. There are two basic correlation relations: positive correlation and negative correlation, defined by the sign of correlation coefficient.[20] The

positive correlation increases the random low frequency noise, whereas the negative correlation decreases the random low frequency noise, compared with the uncorrelated case. The nature of the correlation is determined by defect properties. If both of the defects are Coulomb repulsive defects or Coulomb attractive defects,[24] the RTSs correlation is negative. On the other hand, if one of the defects is Coulomb repulsive and the other is Coulomb attractive, the RTSs correlation is positive. In our experiment here, we observed negative RTS correlation (correlation coefficient $= -0.12 < 0$) resulting from the two correlated Coulomb repulsive defects.

In summary, although most observed random telegraph signals follow the Poisson statistics and exhibit independent uncorrelated events, correlated random telegraph signals are occasionally observed in carbon nanotube transistors. The correlation is due to the overlapping of defects' effective areas. The correlated random telegraph signal stimulates a new understanding on noise and switching events induced by single defects. RTS statistics provides not only a new base to noise modeling and noise metrology in nanotransistors but also a probe technology for the electron interaction in the condensed matter physics.

Acknowledgment. Authors thank Prof. Chongwu Zhou for the help in preparing the carbon nanotube transistor samples. This work was in part supported by MARCO Focus Center on Functional Engineered Nano Architectonics (FENA).

References

(1) 2005 International Technology Roadmap for Semiconductors (ITRS).
(2) Hooge, F. N. *Phys. Lett. A* **1969**, *29*, 139.
(3) Cobhen, D. H.; Muzykanskii, B. A. *Phys. Rev. Lett.* **1995**, *75*, 4274 and references herein.
(4) Nicollian, E. H.; Brews, J. R. *MOS (Metal Oxide Semiconductor) Physics and Technology*; John Wiley & Sons, New York, 2002.
(5) Liu, F.; Wang, K. L.; Li, C.; Zhou, C. *IEEE Trans. Nanotechnol.* **2006**, *5*, 441.
(6) Hooge, F. N. *Phys. Lett.* **1969**, *29A*, 139.
(7) Weissman, M. B. *Rev. Mod. Phys.* **1988**, *60*, 537.
(8) Liu, F.; Bao, M.; Kim, H. J.; Wang, K. L.; Liu, X.; Li, C.; Zhou, C. *Appl. Phys. Lett.* **2005**, *86*, 163102.
(9) Kong, J.; Soh, H. T.; Cassell, A. M.; Quate, C. F.; Dai, H. J. *Nature* **1998**, *395*, 878.
(10) Lu, W.; Ji, Z.; Pfeiffer, L.; West, K. W.; Rimberg, A. J. *Nature* **2003**, *423*, 422.
(11) Gustavsson, S.; Leturcq, R.; Simoviè, B.; Schleser, R.; Ihn, T.; Studerus, P.; Ensslin. *Phys. Rev. Lett.* **2006**, *96*, 076605.
(12) Naaman, O.; Aumentado, J. *Phys. Rev. Lett.* **2006**, *96*, 100201.
(13) Sharp spikes are present due to the third defect E. We ignore the effect due to defect E, due to its little contribution to the RTS statistics.
(14) Ross, S. M. *Introduction to Probability Models*, 4th ed.; Academic Press: New York, 1989.
(15) Devore, J.; Peck, R. *Statistics: the exploration and analysis of data*; West Publishing Company: St. Paul, MN, 1986.
(16) Liboff, R. L. *Introductory Quantum Mechanics*, 4th ed.; Addison Wesley: Reading, MA, 2003.
(17) Kirton, M. J.; Uren, M. J.; Collins, S.; Schulz, M.; Karmann, A.; Scheffer, K. *Semicond. Sci. Technol.* **1989**, *4*, 1116.
(18) If a defect is located inside the oxide, the effective interaction area to channel carriers could be smaller than the circle area. The equivalent effective interaction area in this case could be easily achieved.
(19) Ralls, K. R.; Skocpol, W. J.; Jackel, L. D.; Howard, R. E.; Fetter, L. A.; Epworth, R. W.; Tennant, D. M. *Phys. Rev. Lett.* **1984**, *52*, 228.
(20) Wiener, N. *Acta Math.* **1930**, 55, 117.
(21) Khintchine, A. *Math. Ann.* **1934**, *109*, 604.
(22) Weissman, M. B. *Rev. Mod. Phys.* **1988**, *60*, 537.
(23) Dutta, P.; Horn, P. M. *Rev. Mod. Phys.* **1981**, *53*, 497.
(24) Liu, F.; Bao, M.; Wang, K. L.; Zhang, D.; Zhou, C. *Phys Rev. B* **2006**, *74*, 035438.

NL0722774